Angewandte Chemie
Eine Zeitschrift der Gesellschaft Deutscher Chemiker

Supporting Information

CO Binding to the FeV Cofactor of CO-Reducing Vanadium Nitrogenase at Atomic Resolution

*Michael Rohde, Katharina Grunau, and Oliver Einsle**

anie_202010790_sm_miscellaneous_information.pdf

Supporting Information

Table of Contents

Experimental Procedures

Isolation of protein

The component proteins of the vanadium-dependent nitrogenase were isolated from *Azotobacter vinelandii* according to established procedures.[1] Molybdenum-depleted cultures of *A. vinelandii* were grown in vanadium-containing growth medium. Protein isolation was carried out under strict exclusion of dioxygen, in a chamber containing an N_2/H_2 atmosphere (95:5) or using modified Schlenk techniques with N_2 gas. The isolation protocol consisted of two consecutive anion exchange chromatography columns followed by size exclusion chromatography. Pure protein was stored in a buffer containing 100 mM NaCl, 2.5 mM sodium dithionite and 50 mM Tris/HCl buffer at pH 7.4.

Turnover assays with carbon monoxide

CO turnover assays were carried out with an ATP regeneration system. 5 $mg \cdot mL^{-1}$ VnfDKG was combined with 0.5 $mg \cdot mL^{-1}$ VnfH, yielding an approximate 3:1 ratio of the two nitrogenase components for low electron flux turnover. Buffer solutions contained 20 mM Tris/HCl buffer at pH 7.4, 10 mM $MgCl_2$, 15 mM phosphocreatine, 0.125 $mg \cdot mL^{-1}$ phosphocreatine kinase and 25 mM sodium dithionite. Mixtures were sealed in a Wheaton vial and the headspace was replaced with 100 % carbon monoxide. The gas phase was equilibrated with the solution by incubation for 3 min at 30 °C under agitation at 320 rpm in a water bath shaker. CO turnover was initiated by the addition of ATP to a final concentration of 2.5 mM. The samples were given ample time (~ 2 h) for full depletion of ATP under continuous agitation. Carbon monoxide was eventually removed from the headspace prior to crystallization. To obtain the CO-free structure, the CO-turnover sample was concentrated (100 kDa MWCO, Sartorius) and desalted on a G-25 column (GE Healthcare) under gravitational flow. The turnover assay was then repeated with the same component ratio and buffers, but with argon replacing carbon monoxide in the headspace.

Crystallization

Crystallization of VnfDKG was carried out based on previously published conditions in an anoxic chamber under N_2/H_2 atmosphere (95:5) and was further optimized.[2] Sitting drop vapor diffusion-based crystallization trials were conducted in 24-well crystallization plates (Cryschem). $ZnCl_2$ was added to a final concentration of 0.1 mM in turnover samples prior to crystallization. Drops consisted of a mixture of 2 µL of protein solution at a concentration of 10 $mg \cdot mL^{-1}$ and 2 µL of reservoir solution. Reservoir solutions contained 100 mM Tris/HCl at pH 7.5, 30 mM $MgCl_2$, 20 % (*v/v*) of ethylene glycol, 7–12 % (*w/v*) of polyethylene glycol 8000 and 1 mM sodium dithionite. After the first crystals were obtained from initial crystallization plates, 0.5 µL of a diluted microcrystal suspension were added to each drop of subsequent CO-turnover and crystallization trials. This microseeding procedure was applied repeatedly in order to optimize the amount and shape of crystals formed within each drop. Crystals appeared within a day and grew continuously for 2 weeks. After 2 weeks, crystals were harvested with a nylon loop and flash-frozen in liquid nitrogen.

Data Collection, Structure Solution and Refinement

Diffraction data were collected at the Swiss Light Source (Paul Scherrer Institute, Villigen, Switzerland). High-resolution data of the CO-bound state was collected at a wavelength of 0.85 Å using an Eiger 16M detector (Dectris) at beam line X06SA, while the high-resolution data set of the CO-removed state was collected at a wavelength of 0.91 Å using a Pilatus 2M-F detector (Dectris) at beam line X06DA. To obtain the anomalous scattering contribution of sulfur, crystals of both states were measured at the Pilatus 2M-F detector at a wavelength of 2.0 Å (6200 eV), and in order to maximize the multiplicity of the data, 9 datasets were collected at increasing chi angles, in steps of 5°, by using the PRIGo multi-axis goniometer.[3] XDS was used for indexing and integration,[4] and Aimless from the CCP4 suite for merging and scaling of the data.[5] An existing structure of VnfDKG (PDB-entry: 6FEA) served as a starting model, and further adjustments were made using Coot.[6] This included changes at the C-terminus of VnfD, since a Zn^{2+} ion at the surface that was found in the previous turnover structure was missing. The high-resolution electron density map also allowed to identify and assign Tris and ethylene glycol molecules in the crystal that were added to the model. For the CO-bound state, the prior ligand at the Fe2-Fe6 of the VFe cofactor did not sufficiently explain the observed density map peak and was replaced by CO, which led to a clear improvement in the $F_o–F_c$ difference map. Adjustments to $Q176_D$ and $K361_D$ were made. The structure was refined with REFMAC5[7] using anisotropic temperature factors and a ligand dictionary file from the previous published high resolution crystal structure.[8] All figures were generated with PyMOL.[9]

Results and Discussion

The high level of detail provided by the present crystallographic analysis at a resolution of 1.0 Å for the CO adduct of FeV cofactor provides a wealth of direct information regarding the nature and properties of the individual atoms in the structure. Most importantly, the structure shows individual single maxima for each atom, thus fulfilling the criterion for true atomic resolution in crystallography. The present analyses of the CO-bound and turnover states are the most highly resolved that are available for vanadium nitrogenase today and will be instrumental as a future reference for theoretical approaches. Furthermore, the quality of the electron density map is sufficient to show consistent differences in the electron density maxima for carbon *vs.* nitrogen *vs.* oxygen atoms. In the well-defined core region of the enzyme, this allows for the distinction of light atoms (Fig. S1).

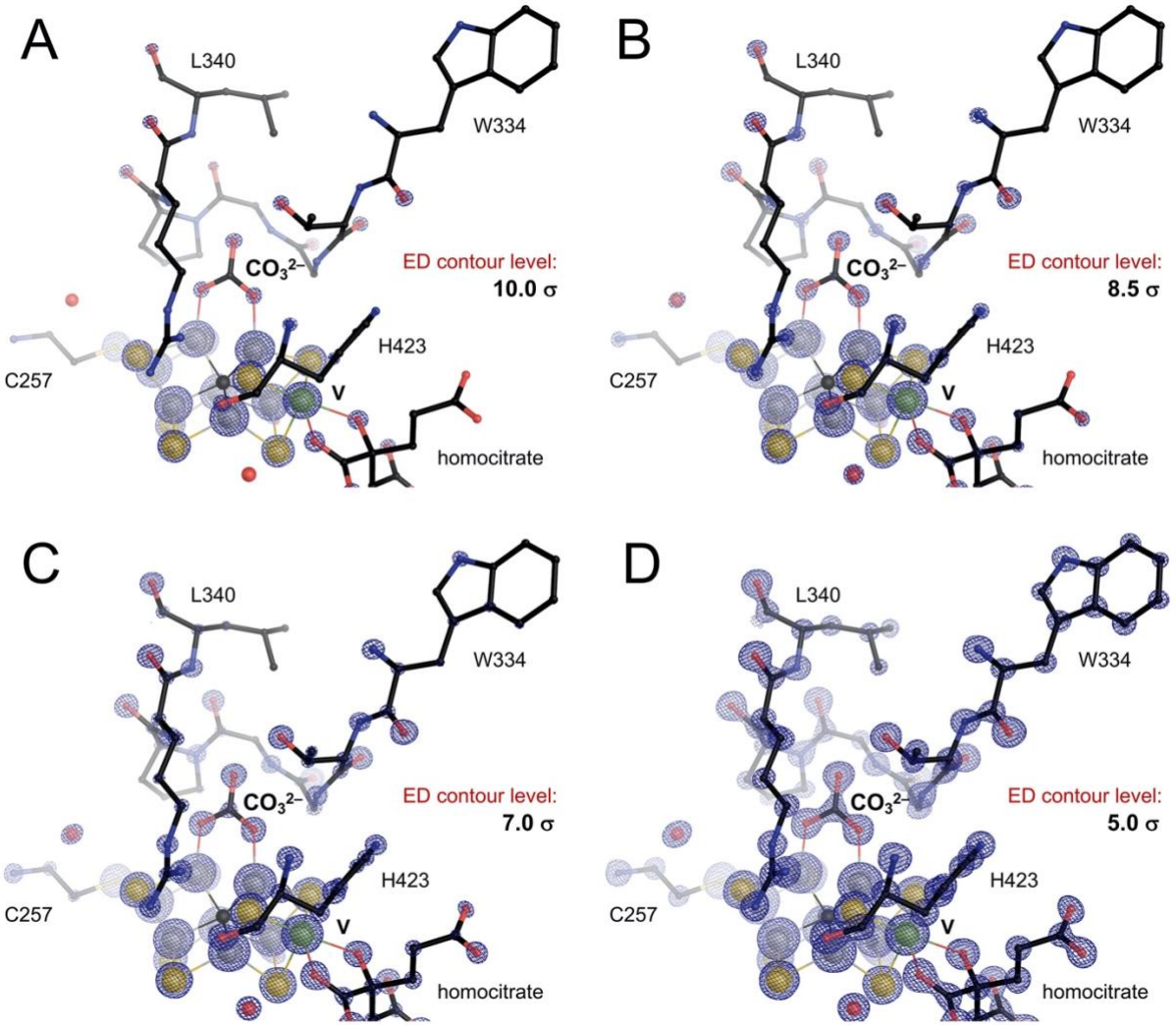

Figure S1. Quality assessment of the electron density maps for the CO adduct of FeV cofactor. At 1.0 Å resolution, the best-defined regions of the map allow for the distinction of C-, N- and O- atoms. **A**) A map contour level of 10 σ level shows maxima for the backbone and carbonate oxygen atoms, as well as for most oxygen atoms of homocitrate, except its flexible ε-carbonyl, but not the crystal water molecules. **B**) At the 8.5 σ level, backbone amide and sidechain nitrogen atom maxima become additionally visible. Note the absence of electron density at the central atom of the carbonate ligand. **C**) Only when contoured at the 7.0 σ level, smaller but distinct maxima for carbon atoms occur. **D**) At the 5 σ level chosen for all figures in the main text, all individual atoms have well-defined, individual electron density maxima as the hallmark of true atomic resolution. The maps in Fig. S1 and S2 are sampled with ½ grid spacing w.r.t. to the figures in the main text.

Notably, as in our previous analysis of the turnover state of V-nitrogenase,[8] we refrain from assigning the nature of the light atom in the CO-removed structure of the enzyme solely based on electron density, even at 1.05 Å resolution (Fig. 4). As seen from anomalous difference maps, we typically find a small fraction of resting state even in turnover state structures that result from inhomogeneous conformations across the entire crystal. A final assignment will ideally include data from separate experiments, in particular EPR spectroscopy.

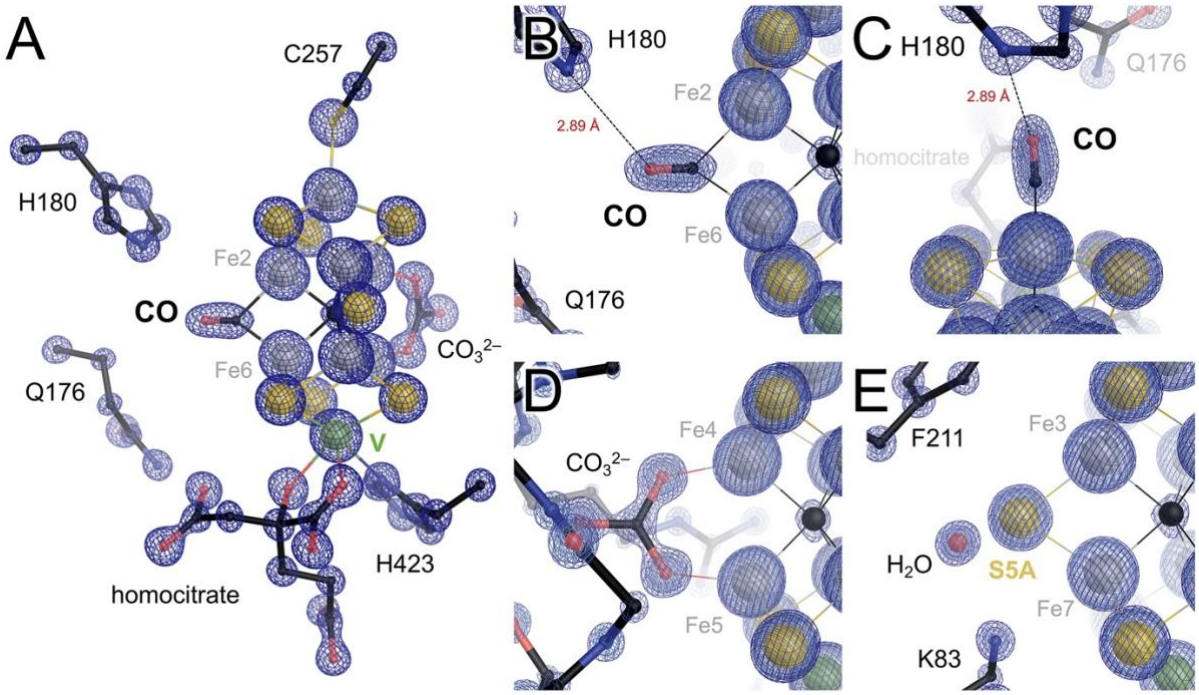

Figure S2. $2F_o–F_c$ difference electron density maps for FeV cofactor at 1.0 Å resolution. **A**) The first ligation sphere of the CO-bound FeV cofactor, with the electron density map (blue mesh) contoured at the 5 σ level. **B**) Detail of the CO ligand coordinated at Fe2 and Fe6 with a hydrogen bond formed to the Nε atom of residue H180. **C**) Detail of the CO ligand viewed along the pseudo-threefold axis of FeV cofactor. **D**) Detail of the carbonate ligand at Fe4 and Fe5 together with the surrounding binding loop. **E**) Detail of the third belt position, where sulfide S5A remains in place and shows a spherical electron density maximum that is highly similar in magnitude to the core sulfides of the cofactor.

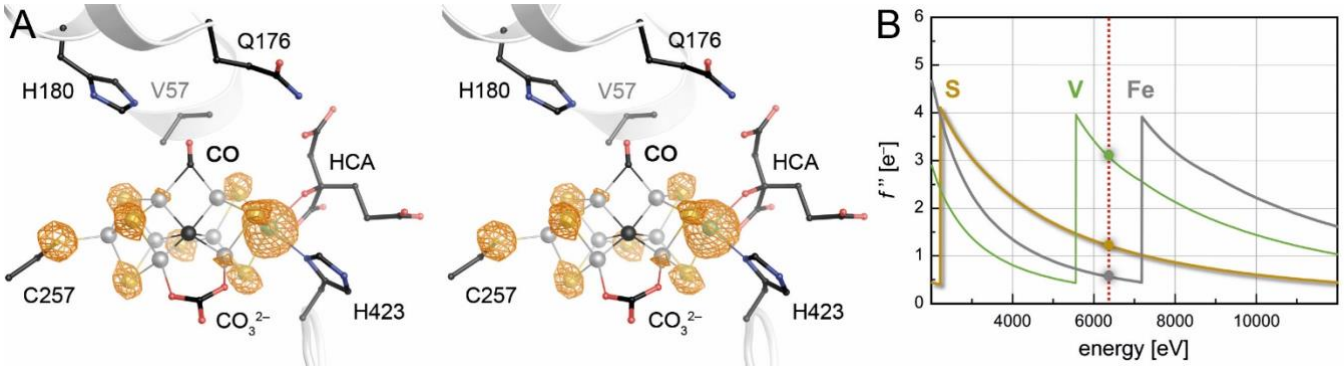

Figure S3. Anomalous difference electron density map for the CO-bound structure of VFe protein. **A**) Stereo image of FeVco with an anomalous difference map. No residual peaks in the map indicate the presence of residual sulfur at either the S2B belt position or in the holding site, indicating that the CO-bound state is very near 100 % occupancy. The diffraction data underlying this map was collected at an X-ray energy of 6200 eV (see Table S1) to 2.0 Å resolution, with an overall multiplicity of 28 for the crystal belonging to space group *P*1. The electron density map is contoured at the 5 σ level. **B**) Plot of anomalous scattering coefficients *f* ” for sulfur, vanadium and iron, displaying the K-edge positions for all elements and highlighting their relative anomalous scattering contributions at 6200 eV, where the data set for panel (A) was collected.

SUPPORTING INFORMATION

At the high resolution of the present analysis, further details with respect to the conformational changes related to CO binding to FeV cofactor became apparent. The rearrangement of residue Q176$_D$ form the CO-bound to the turnover state hinges on an H-bonding interaction of the amide nitrogen N$_{\varepsilon 2}$ with the α-carboxylate of the homocitrate ligand to vanadium. While the length of this bond only shortens from 2.89 Å in the in-conformation to 2.84 Å in the CO-bound out-conformation, the side chain moves towards the organic ligand and displaces residue K361$_D$ that is H-bonded to the α-carboxylate of homocitrate in the in-conformation, but relocates to a weaker (3.02 Å) hydrogen bond to the δ-carboxylate in the out-conformation of residue Q176$_D$ (Fig. S2). Concomitant with this movement, both the amide of Q176$_D$ and the amine of K361$_D$ displace a coordinated water molecule towards a pool of solvent molecules that characteristically fill a cavity adjacent to homocitrate within the protein matrix (Fig. S4). It is tempting to consider that these water molecules may really be product NH$_3$/NH$_4^+$, which – due to an identical number of electrons – could not be distinguished in an electron density map. This arrangement may serve to eject product concomitant with the formation of the inward-facing conformation of the turnover state of the enzyme that can only be attained if a single light atom is bound at Fe2 and Fe6. Notably, K361$_D$ is replaced by a glutamate residue in Mo nitrogenase, but in the absence of a turnover state structure its effect on the solvent structure around FeMo cofactor remains to be determined. We note that Hu and Ribbe recently reported a MoFe protein structure obtained from protein isolated in the absence of reductant that they interpret to reveal multiple N$_2$ binding sites at FeMo cofactor.[10] Although this would represent a substrate-bound state of this nitrogenase variant, the diatomic N$_2$ – like CO in the present work – would not accommodate the glutamine residue in the inward-facing conformation and is thus not a turnover/intermediate state that would inform on side chain flexibility.

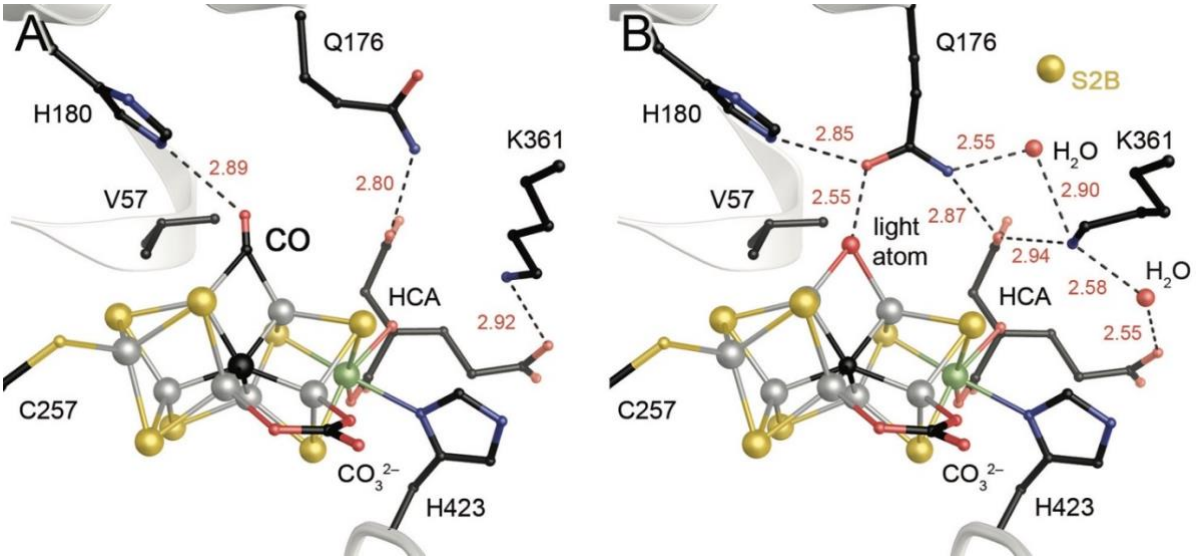

Figure S4. The reorientation of residue K361$_D$ in response to the conformational change of Q176$_D$. **A**) In the CO-bound structure (as well as the resting state of FeV cofactor with sulfide S2B in place at Fe2 and Fe6), K361 forms a hydrogen bond to the δ-carboxylate of the homocitrate ligand, whose α-carboxylate interacts with the amide nitrogen of Q176 in the out-conformation. **B**) In the turnover state obtained after the removal of CO by continuous turnover in the absence of the gas, Q176 is in the in-conformation, forming a much tighter hydrogen-bonding network that involves H180 and the bound light atom at the cluster. Residue K361 also changes its conformation to now interact with the α-carboxylate of homocitrate, creating space for coordinated water (or NH$_4^+$) molecules in close proximity to the cluster.

Table S1. Data collection and refinement statistics

Data Set	CO-bound high resolution	CO-removed high Resolution	CO-bound sulfur anomalous	CO-removed sulfur anomalous
space group	*P*1	*P*1	*P*1	*P*1
cell constants				
a, *b*, *c* [Å]	75.6, 80.0, 107.2	75.6, 80.0, 107.2,	57.7, 80.1, 107.3	75.7, 80.0 ,107.2
α, β, γ [°]	84.1, 72.4, 75.2	84.0, 82.5, 75.0	84.1, 72.5, 75.2	83.9, 72.4, 75.0
wavelength [Å]	0.849205	0.9116	1.9997	2.0000
resolution limit [Å]	48.40 – 1.00 (1.02 – 1.00)	46.62 – 1.05 (1.07 – 1.05)	48.44 – 2.00 (2.13 – 2.00)	48.37 – 2.00 (2.13 – 2.00)
completeness [%]	88.1 (87.5)	94.1 (90.3)	98.1 (86.8)	98.0 (87.0)
anomalous completeness [%]	–	–	96.5 (79.8)	96.5 (79.9)
unique reflections	1,101,498 (53,745)	1,016,322 (48,321)	154,006 (6,754)	153,259 (6,767)
multiplicity [%]	7.6 (7.7)	7.0 (7.4)	28.1 (16.2)	27.9 (16.3)
R_{merge}	0.065 (1.912)	0.084 (2.419)	0.058 (0.219)	0.060 (0.160)
$R_{p.i.m.}$	0.038 (1.112)	0.052 (1.455)	0.016 (0.077)	0.016 (0.056)
mean I/ σ(I)	10.6 (1.0)	10.2 (0.9)	47.6 (11.2)	45.4 (14.7)
$CC_{1/2}$	0.998 (0.592)	0.999 (0.449)	1.000 (0.989)	1.000 (0.993)
refinement statistics				
R_{cryst}	0.1017	0.1186	0.1171	0.1149
R_{free}	0.1168	0.1407	0.1477	0.1451
Cruickshank's DPI	0.0157	0.0199	0.1119	0.1304
figure of merit	0.8781	0.8317	0.9374	0.9404
r.m.s. deviations from ideal values				
bond lengths [Å]	0.0227	0.0245	0.0166	0.0177
bond angles [º]	3.1676	3.2859	2.8105	2.8517

References

[1] D. Sippel, J. Schlesier, M. Rohde, C. Trncik, L. Decamps, I. Djurdjevic, T. Spatzal, S. L. A. Andrade, O. Einsle, *J. Biol. Inorg. Chem.* **2017**, *22*, 161-168.
[2] D. Sippel, O. Einsle, *Nat Chem Biol* **2017**, *13*, 956-960.
[3] S. Waltersperger, V. Olieric, C. Pradervand, W. Glettig, M. Salathe, M. R. Fuchs, A. Curtin, X. Q. Wang, S. Ebner, E. Panepucci, T. Weinert, C. Schulze-Briese, M. T. Wang, *J Synchrotron Radiat* **2015**, *22*, 895-900.
[4] W. Kabsch, *Acta Crystallogr D* **2010**, *66*, 125-132.
[5] M. D. Winn, C. C. Ballard, K. D. Cowtan, E. J. Dodson, P. Emsley, P. R. Evans, R. M. Keegan, E. B. Krissinel, A. G. W. Leslie, A. McCoy, S. J. McNicholas, G. N. Murshudov, N. S. Pannu, E. A. Potterton, H. R. Powell, R. J. Read, A. Vagin, K. S. Wilson, *Acta Crystallogr D* **2011**, *67*, 235-242.
[6] P. Emsley, B. Lohkamp, W. G. Scott, K. Cowtan, *Acta Crystallogr D* **2010**, *66*, 486-501.
[7] G. N. Murshudov, P. Skubak, A. A. Lebedev, N. S. Pannu, R. A. Steiner, R. A. Nicholls, M. D. Winn, F. Long, A. A. Vagin, *Acta Crystallogr D* **2011**, *67*, 355-367.
[8] D. Sippel, M. Rohde, J. Netzer, C. Trncik, J. Gies, K. Grunau, I. Djurdjevic, L. Decamps, S. L. A. Andrade, O. Einsle, *Science* **2018**, *359*, 1484-1489.
[9] L. Schrödinger, **2010**.
[10] W. Kang, C. C. Lee, A. J. Jasniewski, M. W. Ribbe, Y. Hu, *Science* **2020**, *368*, 1381-1385.

Author Contributions

M.R. and O.E. designed experiments, M.R. and K.G. conducted the experiments, M.R., K.G. and O.E. evaluated data, M.R. and O.E. wrote the manuscript, O.E. acquired funding.